Shear deformation capability of different metallic glasses

F.F. Wu and Z.F. Zhang[a)]
Shenyang National Laboratory for Materials Science, Institute of Metal Research,
Chinese Academy of Sciences, Shenyang 110016, China

J. Shen
School of Materials Science and Engineering, Harbin Institute of Technology, Harbin 150001, China

S.X. Mao
Shenyang National Laboratory for Materials Science, Institute of Metal Research, Chinese Academy
of Sciences, Shenyang 110016, China; and Department of Mechanical Engineering and Materials
Science, University of Pittsburgh, Pittsburgh, Pennsylvania 15261

The mechanical properties of $Zr_{52.5}Ni_{14.6}Al_{10}Cu_{17.9}Ti_5$ and $Ti_{40}Zr_{25}Ni_3Cu_{12}Be_{20}$ metallic glasses were investigated under uniaxial compressive loading and small punch loading, respectively. The Zr-based metallic glass displays higher density of shear bands, larger critical shear offsets and higher energy absorbing capability than the Ti-based metallic glass under the small punch tests. A concept of critical shear offset is proposed to explain the difference in shear deformation abilities or plasticity of different metallic glasses. The current experiments demonstrate that, in contrast with the small difference between the responses of the Zr- and Ti-based metallic glasses under uniaxial compressive loading, the biaxial tension produced by the small punch test is an effective way to evaluate the difference in shear deformation abilities and can be used to distinguish the brittleness or plasticity of various metallic glasses.

I. INTRODUCTION

Plastic deformation in metallic glasses (MGs) is still a mystery despite being well investigated.[1–4] Under uniaxial tension, because there are no grain boundaries to stop the fast propagating of shear bands, MGs fail catastrophically, exhibiting near-zero macroscopic plasticity, although the shear band itself has a high microscopic plasticity, up to 10^2–$10^4\%$.[5,6] Under uniaxial compression are also few shear bands, and the specimen fails rapidly by propagation of an individual shear band, displaying only limited plasticity (usually smaller than 2%).[7,8] Although the bending test is considered an inherently stable deformation method because the stress to drive shear bands diminishes gradually as the shear band approaches the neutral axis,[9,10] the ductility-under-bending test can be achieved only if the specimen's dimensions are below a critical value, suggesting a strong size effect on the bending ductility.[11,12] In addition, indentation—especially instrument-driven nanoindentation—has been used extensively to study the evolution of shear bands and plastic deformation instability, i.e., ser-

rated flow behavior, in MGs.[13–15] It was found that dense and regular shear bands were often formed in the region beneath the indenter,[16,17] which is intuitive in understanding the shear band morphology and is useful to investigate the plastic deformation behavior of MGs. In contrast to the catastrophic shear failure under uniaxial compression, MG can display a large inelastic deformation of more than 10% with more shear bands due to confined loading, demonstrating a ductile nature.[18]

Recently, the mechanical properties of MGs under biaxial tensile loading were studied using the small punch test (SPT).[6,19] It was found that MG could be controlled to create regularly arrayed fine multiple shear bands under the SPT, indicating that MG essentially has a good plastic deformation capability—and thus high ductility—under suitable loading conditions. The findings show that the initiation and propagation of shear bands in MG strongly depend on the stress state. Herein, by using the SPT, shear deformation behaviors of different MGs under biaxial tension are evaluated and analyzed. We confirm that there exist great differences in the shear deformation capabilities of various MGs, which provides an effective method to distinguish their brittleness or plasticity.

II. EXPERIMENTAL

Zr- and Ti-based MGs with nominal chemical compositions of $Zr_{52.5}Ni_{14.6}Al_{10}Cu_{17.9}Ti_5$ and

$Ti_{40}Zr_{25}Ni_3Cu_{12}Be_{20}$ were prepared by arc melting. The final ingots have a rectangular shape with a dimension of $60 \times 30 \times 3$ mm^3. The microstructure was characterized by a Rigaku x-ray diffractometer (XRD) with Cu Kα radiation. XRD patterns showed that the as-cast alloy had a fully glassy structure. Mechanical properties of the two MGs were characterized using uniaxial compression and the SPT technique.[6] Dimensions of the rectangular specimens for uniaxial compression are $3 \times 3 \times 6$ mm^3. In addition, SPT specimens—0.7 mm thick and 10 mm in diameter—were cut from the two kinds of MG ingots with an electric spark cutting machine and were then ground and polished to a thickness of 0.3–0.5 mm with a 2.5-μm abrasive paste. All mechanical tests were performed with an MTS810 testing machine at room temperature. After testing, all the specimens were observed with a Leo Supra 35 scanning electron microscope (SEM) and an Olympus LEXT OLS3000 laser confocal scanning microscope (LCSM) to reveal the deformation and fracture features and quantitatively measure the length of the shear offset.

III. RESULTS AND DISCUSSION

Figure 1 shows the compressive stress–strain curves of Zr- and Ti-based MGs at a constant strain rate of 1×10^4 s^{-1}. The Zr-based MG displays an initial elastic deformation behavior with an elastic strain of about 1.8%, and its elastic modulus is about 82.7 GPa. It then begins to yield at a stress of 1.6 GPa, followed by a serrated flow with a stress amplitude of about 25 MPa. The fracture strength is 1.7 GPa, and a compressive plastic strain of 0.5% is achieved before fracture. From the upper left inset of Fig. 1, it can be seen that the Zr-based MG failed with a shear fracture angle of 42°, and the

fracture surface is characterized by vein patterns, which is consistent with an earlier report.[8] As for the Ti-based MG, its elastic strain, compressive plastic strain, elastic modulus, and fracture strength are 1.8%, 0.1%, 88.9 GPa, and 1.8 GPa, respectively. Its shear fracture angle is about 41°, and its fracture surface is similar to that of the Zr-based MG, displaying typical vein patterns (see lower right inset, Fig. 1). From the results above, the two MGs display similar mechanical properties under compressive loading.

From the load–deflection curves (Fig. 2) produced by the SPT, it is seen that the maximum deflection of the Zr-based MG at fracture is 1.4 mm with a load of 3.4 kN. However, for the Ti-based MG, the maximum deflection at fracture and the corresponding load are 0.6 mm and 1.7 kN, which are only half of those for the Zr-based MG. SEM observations show that multiple intersected radial and circumferential shear bands are regularly formed on the lower surfaces of the two MGs, as displayed in Figs. 3(a), 3(b), 3(d), and 3(e). The radial and circumferential shear offsets are respectively 17.3 and 26.6 μm for the Zr-based MG, obviously larger than those (11.6 and 7.4 μm) for the Ti-based MG [see Figs. 3(a) and 3(d) and summary in Table I]. For the Zr-based MG, the densities of the radial and circumferential shear bands are 3.8×10^5 m^{-1} and 83.4 rad^{-1}, respectively, which are obviously higher than those (2.1×10^5 m^{-1} and 35.7 rad^{-1}) for the Ti-based MG (see Table I). From the load–deflection curves in Fig. 2 and the SEM observations in Fig. 3, it can be concluded that the global plasticities do occur in the two MGs under the SPT and can be approximately expressed as

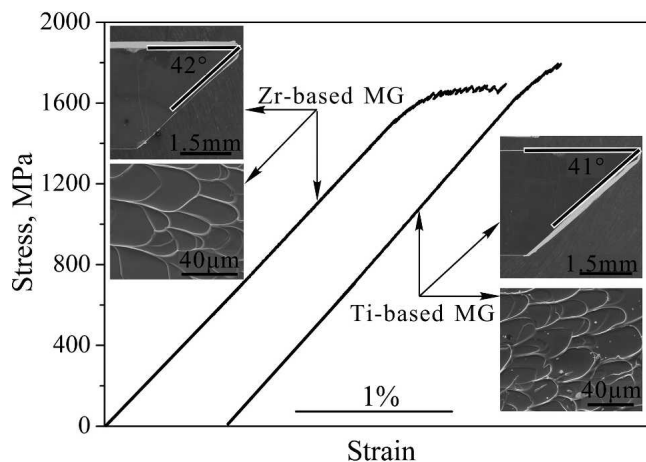$$\epsilon_p = \frac{\sqrt{r^2 + f^2} - r}{r} \quad , \qquad (1)$$

FIG. 1. Compressive stress–strain curves of Zr- and Ti-based MGs. Left upper insets are the SEM images of the lateral and fracture surface for the Zr-based MG; right lower insets are those for the Ti-based MG.
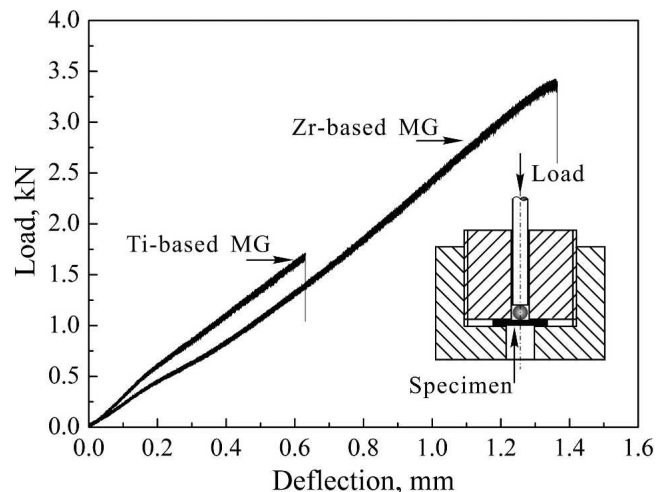

FIG. 2. Load–deflection curves of the Zr- and Ti-based MGs. (Inset) Schematic illustration of the clips for the small punch test.
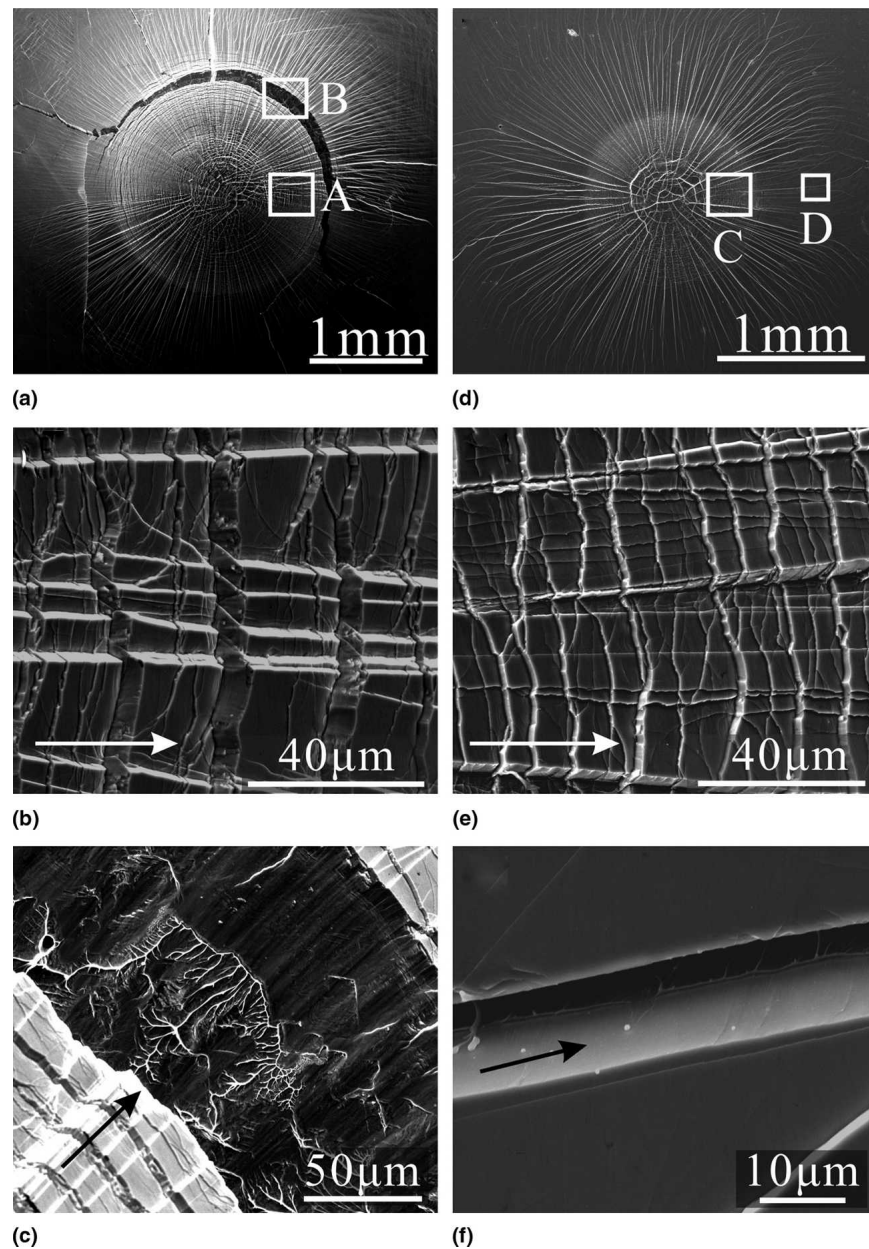
FIG. 3. (a) SEM image of the lower surface of the Zr-based MG specimen after the small punch test. (b, c) High-resolution SEM images of regions A and B in (a), showing the profuse multiple shear bands and fracture features, respectively. (d) SEM image of the lower surface of the Ti-based MG specimen after the small punch test. (e, f) High-resolution SEM images of regions C and D in (d), displaying the shear bands and fracture features. Arrow denotes the radial direction.

where *r* is the effective specimen radius, i.e., the radius of the low die of the small punch clip, and *f* is the deflection of the specimen at central position up to fracture. In Eq. (2), the global plasticities of the Zr- and Ti-based MGs were estimated to be about 13.8% and 3.1%, which are far larger than those (0.5% and 0.1% for Zr- and Ti-based MGs, respectively, as shown in Fig. 1) achieved by the uniaxial compression tests. It is noted that the global plasticity calculated from Eq. (1) is different from the equivalent plastic strain as proposed in our recent study.[19] The global plasticity is a mean value in the whole deformed region, but the equivalent strain can be calculated at different positions and has the maximum value at the necking region. Therefore, the global plasticity is smaller than the equivalent plastic strain at necking region.

As is well known, the room-temperature plastic strain of MG is produced by the shear offset of two undeveloped parts separated by the localized shear band.[20] With the shear band propagating, the shear offset increases, resulting in the macro-scale plastic strain. When a shear band propagates to a critical length, it

TABLE I. Mechanical properties and analysis data of shear bands for Zr- and Ti-based MGs under biaxial tension load by the small punch test.

Composition of MGs	Range of shear band (mm)		Density of shear band		Shear offset (μm)	
	Radial direction	Circumferential direction	Radial direction (m^{-1})	Circumferential direction (rad^{-1})	Radial direction	Circumferential direction
$Zr_{52.5}Ni_{14.6}Al_{10}Cu_{17.9}Ti_5$	2.05	3.77	3.8×10^5	83.4	17.3	26.6
$Ti_{40}Zr_{25}Ni_3Cu_{12}Be_{20}$	1.20	3.03	2.1×10^5	35.7	11.6	7.4

develops maturely with a low bonding strength,[3] leading to the final catastrophic fracture along shear band. Thus, there should be a "critical shear offset (λ_c)" above which the shear band starts to be unstable, leading to the final shear fracture.[6] The critical shear offset is a direct parameter phenomenally reflecting the stable shear capability. In principle, the length of the critical shear offset is equal to the width of the smooth region at the initial fracture surface of metallic glass sample after deformation.[6,21] Therefore, it is suggested that the shear deformation capability of metallic glass is related to the critical shear offset: the plastic strain of metallic glass at fracture increases linearly with increasing critical shear offset. Furthermore, based on the concept of the critical shear offset, the overall deformation behavior of metallic glass can be categorized into two regimes with regard to the sample size. At first, if the sample size w is significantly larger than the critical shear offset (λ_c), the shear offset produced by propagation of shear band will reach the critical one (λ_c), and catastrophic failure will occur. Based on the results above, it is found that the critical shear offset λ_c is an important parameter controlling the compatibility of deformation, the ductility of MG, and the failure modes.[22] Since the deformation energy represents a capability to absorb the plastic work applied to a material, it can be considered as one of the effective methods to evaluate the deformation capability of the Zr- and Ti-based MGs. Under the SPT, the total plastic deformation work of an MG sample can be divided into radial and circumferential ones, respectively, i.e.,

$$W_P = W_R + W_C \quad , \tag{2a}$$

$$W_R = N_R \int_0^{\lambda_R} F_R d\lambda \quad , \tag{2b}$$

$$W_C = N_C \int_0^{\lambda_C} F_C d\lambda \quad , \tag{2c}$$

where W_R is the plastic energy absorbed by the radial shear bands, W_C is the plastic energy absorbed by the circumferential shear bands, N_R is the number of radial shear bands, N_C is the number of circumferential shear bands, F_R is the force forming the radial shear bands, F_C is the force forming the circumferential shear bands, λ_R is the radial shear offset, and λ_C is the circumferential shear offset. According to the uniaxial compressive properties, the shear stress forming shear bands in Zr- and Ti-based MGs can be considered to be similar because

they have approximately equal strength. However, the number of the shear bands and the shear offsets of Zr-based MG are larger than those of Ti-based MG (see Fig. 3 and Table I). Therefore, the total plastic work of Zr-based MG is far larger than that of Ti-based MG, i.e., $W_P^{Zr} > W_P^{Ti}$ indicating that the Zr-based MG possesses higher ductility than the Ti-based MG under the SPT.

Figures 3(c) and 3(f) show typical fracture features for the Zr- and Ti-based MGs, it can be seen that the Zr-based MG failed by the circumferential shear fracture, but the Ti-based MG failed by the radial shear fracture, displaying a different failure mode even under the same loading conditions. However, differences in the failure modes of different MGs are difficult to distinguish in detail under uniaxial compression loading.[19] Based on the concept of critical shear offset λ_c, a failure map of different MGs can be drawn, as shown in Fig. 4. Three types of failure modes correspond with the three types of MGs. For the type I MGs, the critical shear offset λ_c is as high as 50–70 μm, they can undergo severe shear deformation with highly dense shear bands formed in both circumferential and radial directions on the SPT specimen, and final failure occurs in the circumferential direction on the specimen [see inset (a) of Fig. 4]. The
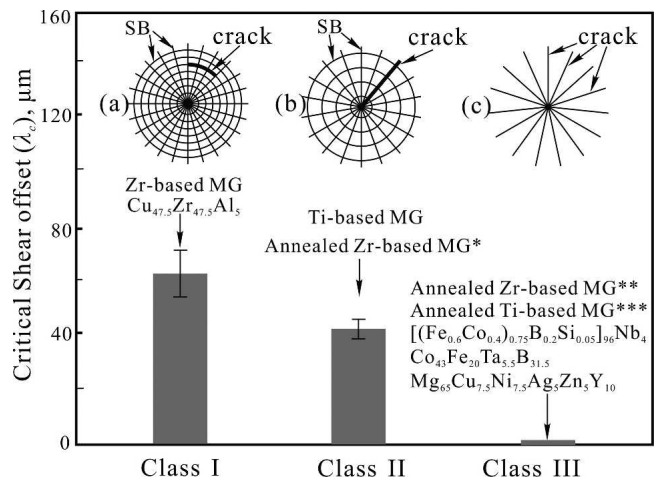

FIG. 4. Illustration of failure modes map by taking into account the critical shear offsets in different MGs. Insets a, b, and c are three typical morphologies of shear bands (SB) and failure modes correspondent to the three kinds of MGs. *Present Zr-based MG annealed at 653 K for 1 h; **present Zr-based MG annealed at 693 K for 1 h; ***present Ti-based MG annealed at 653 K for 1 h.

present Zr-based MG and $Cu_{47.5}Zr_{47.5}Al_5$ MG[6,23] should belong to this type. For the type II MGs, the critical shear offset and the density of shear bands are relatively smaller than those of the type I MGs; though they can undergo certain shear deformation, they fail quickly by shear crack in the radial direction [see inset (b) of Fig. 4]. The present Ti- and the Zr-based MGs annealed at 623 K for 1 h[19] are type II MGs. Finally, it is also observed that some MGs have almost zero shear deformation capability (critical shear offset λ_c is close to zero), and they fail by normal fracture in the radial direction (see right inset in Fig. 4), such as the present Zr-based MG annealed at 693 K for 1 h,[19] the present Ti-based MG annealed at 653 K for 1 h, $[(Fe_{0.6}Co_{0.4})_{0.75}B_{0.2}Si_{0.05}]_{96}Nb_4$,[24,25] $Co_{43}Fe_{20}Ta_{5.5}B_{31.5}$,[25,26] and $Mg_{65}Cu_{7.5}Ni_{7.5}Ag_5Zn_5Y_{10}$.[25,27] These MGs all displayed brittle features even under uniaxial compression loading, for example, failure in a fragmentation mode.[28–30] Such MGs should correspond to the type III MG (Fig. 4), if their shear deformation capability is taken into account.

In summary, both Zr- and Ti-based MGs exhibit similar shear deformation and fracture modes under uniaxial compression; however, they display absolutely different failure modes under biaxial tension when subjected to the SPT. For most MG materials, it is clearly shown that there are three types of failure modes under the SPT, i.e., normal, radial, and circumferential shear failures, which are controlled by the shear deformation capability (critical shear offset λ_c) of the different MGs.

ACKNOWLEDGMENTS

REFERENCES

1. C.A. Schuh, T.C. Hufnagel, and U. Ramamurty: Mechanical behavior of amorphous alloys. *Acta Mater.* **55,** 4067 (2007).

2. M. Chen, A. Inoue, W. Zhang, and T. Sakurai: Extraordinary plasticity of ductile bulk metallic glasses. *Phys. Rev. Lett.* **96,** 245502 (2006).

3. H. Bei, S. Xie, and E.P. George: Softening caused by profuse shear banding in a bulk metallic glass. *Phys. Rev. Lett.* **96,** 105503 (2006).

4. Z.F. Zhang, H. Zhang, X.F. Pan, J. Das, and J. Eckert: Effect of aspect ratio on the compressive deformation and fracture behaviour of Zr-based bulk metallic glass. *Philos. Mag. Lett.* **85,** 513 (2005).

5. H. Chen, Y. He, G.J. Shiflet, and S.J. Poon: Deformation-induced nanocrystal formation in shear bands of amorphous alloys. *Nature* **367,** 541 (1994).

6. F.F. Wu, Z.F. Zhang, F. Jiang, J. Sun, J. Shen, and S.X. Mao: Multiplication of shear bands and ductility of metallic glass. *Appl. Phys. Lett.* **90,** 191909 (2007).

7. W.J. Wright, R. Saha, and W.D. Nix: Deformation mechanisms of the $Zr_{40}Ti_{14}Ni_{10}Cu_{12}Be_{24}$ bulk metallic glass. *Mater. Trans.* **42,** 642 (2001).

8. Z.F. Zhang, J. Eckert, and L. Schultz: Difference in compressive and tensile fracture mechanisms of $Zr_{59}Cu_{20}Al_{10}Ni_8Ti_3$ bulk metallic glass. *Acta Mater.* **51,** 1167 (2003).

9. R.D. Conner, Y. Li, W.D. Nix, and W.L. Johnson: Shear band spacing under bending of Zr-based metallic glass plates. *Acta Mater.* **52,** 2429 (2004).

10. R.D. Conner, W.L. Johnson, N.E. Paton, and W.D. Nix: Shear bands and cracking of metallic glass plates in bending. *J. Appl. Phys.* **94,** 904 (2003).

11. A. Inoue, A. Katsuya, K. Amiya, and T. Masumoto: Preparation of amorphous Fe–Si–B and Co–Si–B alloy wires by a melt extraction method and their mechanical and magnetic properties. *Mater. Trans., JIM* **36,** 802 (1995).

12. A. Katuya, A. Inoue, and K. Amiya: Production of Ni–Si–B amorphous alloy wires by melt extraction and their thermal and mechanical properties. *Int. J. Rapid Solidif.* **9,** 137 (1996).

13. C.A. Schuh and T.G. Nieh: A nanoindentation study of serrated flow in bulk metallic glasses. *Acta Mater.* **51,** 87 (2003).

14. W.H. Jiang, F.E. Pinkerton, and M. Atzmon: Mechanical behavior of shear bands and the effect of their relaxation in a rolled amorphous Al-based alloy. *Acta Mater.* **53,** 3469 (2005).

15. B. Yang and T.G. Nieh: Effect of the nanoindentation rate on the shear band formation in an Au-based bulk metallic glass. *Acta Mater.* **55,** 295 (2007).

16. U. Ramamurty, S. Jana, Y. Kawamura, and K. Chattopadhyay: Hardness and plastic deformation in a bulk metallic glass. *Acta Mater.* **53,** 705 (2005).

17. H.W. Zhang, X.N. Jing, G. Subhash, L.J. Kecskes, and R.J. Dowding: Investigation of shear band evolution in amorphous alloys beneath a Vickers indentation. *Acta Mater.* **53,** 3849 (2005).

18. J. Lu and G. Ravichandran: Pressure-dependent flow behavior of $Zr_{41.2}Ti_{13.8}Cu_{12.5}Ni_{10}Be_{22.5}$ bulk metallic glass. *J. Mater. Res.* **18,** 2039 (2003).

19. F.F. Wu, Z.F. Zhang, J. Shen, and S.X. Mao: Shear deformation and plasticity of metallic glass under multiaxial loading. *Acta Mater.* **56,** 894 (2008).

20. C.A. Pampillo: Review: Flow and fracture in amorphous alloys. *J. Mater. Sci.* **10,** 1194 (1975).

21. C.A. Pampillo and H.S. Chen: Compressive plastic deformation of a bulk metallic glass. *Mater. Sci. Eng., A* **13,** 181 (1974).

22. F.F. Wu, Z.F. Zhang, and S.X. Mao: Size-dependent shear fracture and global tensile plasticity of metallic glasses. *Acta Mater.* (2008, in press).

23. J. Das, M.B. Tang, K.B. Kim, R. Theissmann, F. Baier, W.H. Wang, and J. Eckert: "Work-hardenable" ductile bulk metallic glass. *Phys. Rev. Lett.* **94,** 205501 (2005).

24. A. Inoue, B.L. Shen, and C.T. Chang: Super-high strength of over 4000 MPa for Fe-based bulk glassy alloys in $[(Fe_{1-x}Co_x)_{0.75}B_{0.2}Si_{0.05}]_{(96)}Nb_4$ system. *Acta Mater.* **52,** 4093 (2004).

25. F.F. Wu, Z.F. Zhang, B.L. Shen, S.X. Mao, and J. Eckert: Size effect on shear fracture and fragmentation of a $Fe_{57.6}Co_{14.4}B_{19.2}Si_{4.8}Nb_4$ bulk metallic glass. *Adv. Eng. Mater.* **10,** 727 (2008).

26. A. Inoue, B.L. Shen, H. Koshiba, H. Kato, and A.R. Yavari: Ultra-high strength above 5000 MPa and soft magnetic properties of Co–Fe–Ta–B bulk glassy alloys. *Acta Mater.* **52,** 1631 (2004).

27. Y.K. Xu, H. Ma, J. Xu, and E. Ma: Mg-based bulk metallic glass composites with plasticity and gigapascal strength. *Acta Mater.* **53,** 1857 (2005).

28. Q.J. Chen, J. Shen, D.L. Zhang, H.B. Fan, and J.F. Sun: Mechanical performance and fracture behavior of $Fe_{41}Co_7Cr_{15}Mo_{14}Y_2C_{15}B_6$ bulk metallic glass. *J. Mater. Res.* **22,** 358 (2007).

29. Z.F. Zhang, H. Zhang, B.L. Shen, A. Inoue, and J. Eckert: Shear fracture and fragmentation mechanisms of bulk metallic glasses. *Philos. Mag. Lett.* **86,** 643 (2006).

30. G. Chen and M. Ferry: Some aspects of the fracture behaviour of $Mg_{65}Cu_{25}Y_{10}$ bulk metallic glass during room-temperature bending. *J. Mater. Sci.* **41,** 4643 (2006).